Structural Insights into the Interaction Between Testis-Specific Y-Encoded-Like Protein 5 and Ubiquitin-Specific Protease 7

Marine Ancia[1,2], Khadija Wahni[3,4,5], Joudy Chakrowf[1], Asia El Aakchioui[1], Eloïse Claude[2], Guillaume de Lhoneux[2], Maxime Liberelle[1#], Steven Janvier[3,5], Ekaterina Baranova[3,4,5], Julia Malo Pueyo[3,4,5], Ariana Jijon Vergara[1], Nicolas Papadopoulos[7,8], Clémence Balty[7,9], Jérôme Dejeu[6], Anabelle Decottignies[2], Joris Messens[3,4,5]* and Raphaël Frédérick[1]*

1. Medicinal Chemistry Research Group, Louvain Drug Research Institute, Université catholique de Louvain, B-1200 Brussels, Belgium
2. Genetic and Epigenetic Alterations of Genomes, de Duve Institute, Faculty of Pharmacy and Biomedical Sciences, Université catholique de Louvain, Brussels 1200, Belgium
3. VIB-VUB Center for Structural Biology, Vlaams Instituut Voor Biotechnologie, B-1050 Brussels, Belgium
4. Brussels Center for Redox Biology, Vrije Universiteit Brussel, B-1050 Brussels, Belgium
5. Structural Biology Brussels, Vrije Universiteit Brussel, B-1050 Brussels, Belgium
6. Université Marie et Louis Pasteur, SUPMICROTECH, CNRS, institut FEMTO-ST, 25000 Besançon, France
7. de Duve Institute, Université catholique de Louvain, Brussels, Belgium
8. Ludwig Institute for Cancer Research, Brussels, Belgium

9. IONS/NEUR, Université Catholique de Louvain, Brussels, Belgium

#. Present address: University of Lille, Lille Neurosciences and Cognition Research Center, U1172, Lille, France

* Corresponding authors:

Raphaël Frédérick (raphael.frederick@uclouvain.be) (+32 2 7647341)

Joris Messens (Joris.Messens@vub.be) (+32 2 6291992)

Running title: Structural Insights into the TSPYL5-USP7 Interaction

Table of content:

Manuscript pages: 1-39

Supplementary material pages: S1-S28

Figures: Fig. 1 - Fig. 5

TSPYL5-USP7-supplementary-material: Complementary results about immunoprecipitation assay, mass spectrometry experiments, structure prediction, hydrogen-deuterium exchange mass spectrometry experiments, proteins production and analysis, BioLayer Interferometry assay, peptides screening, sequence comparison and hotspots localization, dynamic light scattering and mass photometry experiments, and Materials and Methods Tables.

ABSTRACT

The Alternative Lengthening of Telomeres (ALT) mechanism enables telomere maintenance, contributing to the immortality of certain cancer cells. Disrupting the interaction between Testis-Specific Y-encoded-like Protein 5 (TSPYL5) and Ubiquitin-Specific Protease 7 (USP7) has emerged as a promising strategy to target ALT-dependent cancers. While the N-terminal MATH domain of USP7 mediates the protein interaction, the regions of TSPYL5 involved in binding remain unclear. Here, we present a structural analysis of the TSPYL5-USP7 interaction to guide targeted therapeutic strategies. We showed that TSPYL5 is intrinsically disordered, with an unfolded N-terminal region and partial structure in the C-terminal half. *In vitro*, recombinantly expressed TSPYL5 binds USP7 with nanomolar affinity and was prone to C-terminal truncation. However, the truncated form retained a similar binding affinity for USP7, suggesting the primary interaction site resides in the N-terminal region of TSPYL5. We identified three key binding hotspots within TSPYL5: residues 65-97, residues 210–262, and residues 368–388. Moreover, TSPYL5 forms trimers that further assemble into hexamers. This study provides the first structural and quantitative analysis of the TSPYL5-USP7 interaction, highlighting these three binding sites. These findings lay the groundwork for the development of novel inhibitors targeting ALT-dependent cancers.

Keywords:

ALT mechanism, cancer, co-immunoprecipitation, microscale thermophoresis, biolayer interferometry, hydrogen-deuterium exchange mass spectrometry, peptides screening, AlphaFold, mass photometry, electron microscopy

A 50-75-word statement, written for a broader audience, outlining the importance and/or impact of the work presented in the manuscript:

The interaction between TSPYL5 and USP7 is critical for the survival of cancer cells that use the Alternative Lengthening of Telomeres (ALT) mechanism for telomere maintenance —common in many solid pediatric tumors. By identifying key regions involved in this interaction, our findings offer a foundation for developing targeted therapies that could disrupt ALT in cancer cells, providing a promising new approach for treating these challenging cancers.

INTRODUCTION

Cellular immortality, a hallmark of cancer (Hanahan and Weinberg 2011), is often achieved through the maintenance of telomere length. Cancer cells typically utilize one of two primary mechanisms for telomere elongation: the reactivation of telomerase via the re-expression of the *hTERT* telomerase gene, or the activation of the Alternative Lengthening of Telomeres (ALT) mechanism, which involves homologous recombination-based telomere maintenance (Claude and Decottignies 2020; Zhang and Zou 2020).

While telomerase is reactivated in approximately 85% of cancers, ALT is particularly prevalent in certain tumor types, such as sarcomas, neuroblastomas, and central nervous system tumors, where it occurs in 50-60% of cases. Importantly, around one-third of solid pediatric tumors are ALT-dependent (Claude and Decottignies 2020). Current pediatric cancer treatments often cause severe side effects because of their aggressiveness and non-specificity (Forrest et al. 2018). Targeting ALT offers a promising strategy for developing more specific and less toxic therapies, as the pathway is inactive in normal cells. However, therapeutic interventions targeting ALT remain challenging, as this pathway relies on canonical homologous recombination DNA repair pathways, which complicates the development of selective inhibitors. Despite these difficulties, several key features of ALT are being investigated as potential targets (Zhang and Zou 2020).

The Testis-Specific Y-encoded-like Protein 5 (TSPYL5) recently emerged as a putative therapeutic target against ALT-positive (ALT^+) tumors, as it is essential for the survival of ALT^+ cells, including SV40T-immortalized fibroblasts and sarcoma cells (Episkopou et al. 2019). Depletion of TSPYL5 selectively induces ALT^+ cell death, without affecting

the viability of telomerase-positive cells or normal skin fibroblasts, providing a strong rationale for targeting this protein in ALT^+ tumors (Episkopou et al. 2019). Mechanistically, ALT^+ cell death induced by TSPYL5 depletion was found to result from the interaction of TSPYL5 with the Ubiquitin-Specific Protease 7 (USP7). The depletion of TSPYL5 leads to the degradation of the Protection of Telomeres 1 (POT1) component of the shelterin complex, triggering DNA damage responses and cell death (Episkopou et al. 2019). Given the importance of the TSPYL5-USP7 interaction in ALT^+ cancer cell survival, targeting this protein-protein interaction represents an attractive therapeutic strategy for ALT-dependent cancers.

USP7, a deubiquitinating enzyme, is known to interact with TSPYL5 through its TRAF-like or MATH domain (Epping et al. 2011), but the interacting region of TSPYL5 remains unknown. TSPYL5, a member of the TSPY-like protein family, is characterized by a high degree of intrinsic disorder (65.7% of predicted intrinsically disordered regions (IDRs)), which likely contributes to its propensity for liquid-liquid phase separation (LLPS) (Silonov et al. 2024). Evidence suggests its involvement in various cellular functions, such as nucleosome assembly (Dalui et al. 2022) or modulation of p53 levels (Epping et al. 2011). However, the structural features of TSPYL5 and how it interacts with USP7 remain poorly explored.

In this study, we sought to identify the key interaction sites between TSPYL5 and USP7. By characterizing the structural properties of TSPYL5, quantifying its binding affinity for USP7, and mapping the interacting regions through cellular assays and peptide screening, we aim to provide crucial insights that could guide the development of targeted therapies to disrupt this interaction, offering a promising approach for treating ALT-dependent pediatric tumors.

RESULTS

The N-terminal region of TSPYL5 interacts with USP7 in pull-down assays

To study the TSPYL5-USP7 interaction and identify potential binding hotspots on TSPYL5, we designed constructs for the overexpression of either full-length TSPYL5 (FL) or three distinct segments of TSPYL5 in human cells. The last 174 amino acids of TSPYL5, predicted to form a NAP-like domain, were included in TSPYL5 #3 (residues 243–417) (Fig. 1A-B). The remaining sequence was divided into two regions: TSPYL5 #1 (residues 1–123), corresponding to the N-terminal part predicted to be unfolded, and TSPYL5 #2 (residues 124–242), which includes the remaining unfolded region and a predicted α-helix (Fig. 1A-B). Each construct (FL, #1, #2, and #3) was fused to an N-terminal triple-Flag tag (Fig. 1A).

Flag immunoprecipitation assays were performed using lysates from U2OS cells (Fig. 1C) or HEK293T cells (Fig. S1) overexpressing these constructs. As expected, Flag-TSPYL5 FL efficiently co-immunoprecipitated USP7, confirming their interaction. Flag-TSPYL5 #1 also pulled down USP7, indicating that this part of TSPYL5 mediates the interaction. Additionally, Flag-TSPYL5 #2, which includes the predicted α-helix, also recovered USP7, indicating an additional interaction site within this region. In contrast, Flag-TSPYL5 #3, corresponding to the C-terminal region, failed to pull down USP7 (Fig. 1C). These findings suggest that the C-terminal region of TSPYL5 does not participate in USP7 binding, while the N-terminal part plays a key role in the interaction.

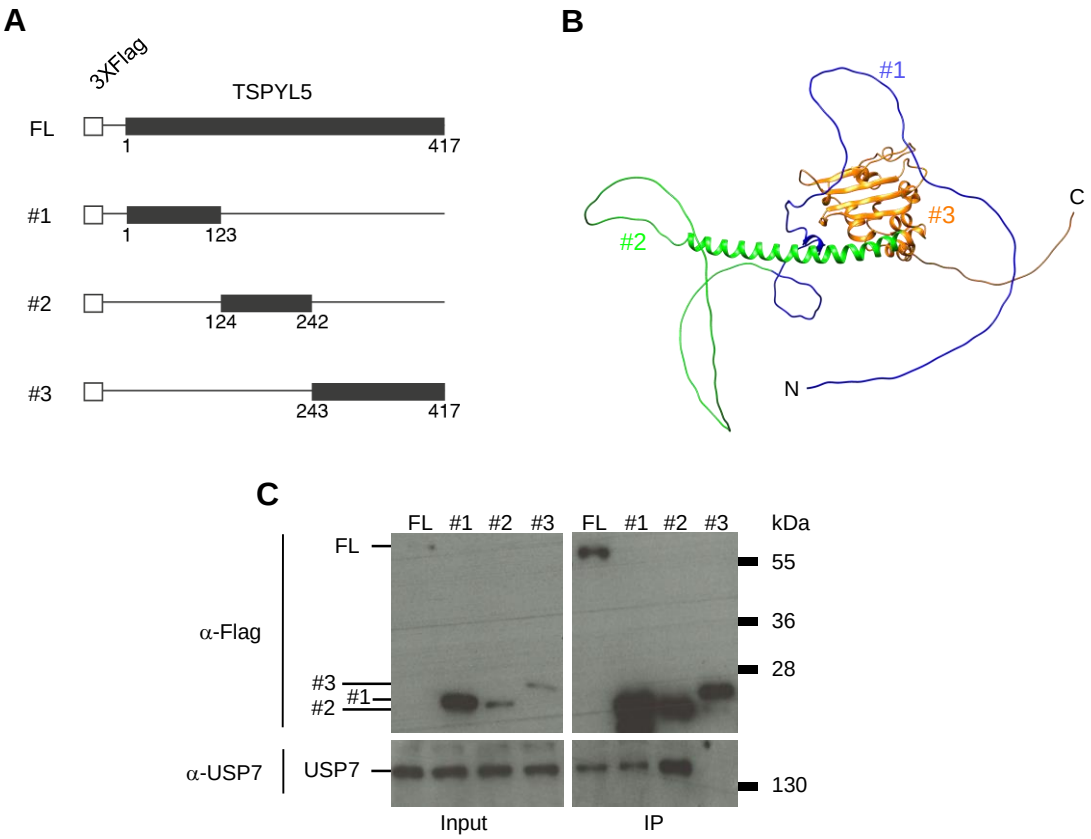

Figure 1: The N-terminal region of TSPYL5 drives the interaction with USP7 in a cellular model. (**A**) Schematic representation of TSPYL5 protein constructs used in this study: FL represents the full-length TSPYL5 sequence; #1 includes amino acids 1–123, #2 includes amino acids 124–242, and #3 includes amino acids 243–417. Each TSPYL5 construct is fused with a triple Flag tag for interaction analysis. (**B**) AlphaFold2-predicted structural model of TSPYL5, illustrating the distinct regions defined in (A): #1 in blue, #2 in green and #3 in orange. “N” refers to the N-terminal end and “C” to the C terminal end of the sequence. (**C**) Lysates of U2OS cells transfected with plasmids encoding Flag-TSPYL5 FL, #1, #2 or #3, as defined in (A), were subjected to immunoprecipitation (IP) using an anti-Flag antibody, followed by western blotting (WB). "Input" refers to total cellular lysates, and "IP" represents proteins pulled down by anti-Flag antibody. WB detection was performed using either anti-Flag (α-Flag) or anti-USP7 (α-USP7) antibodies.

TSPYL5 is a partially folded protein

To further investigate the TSPYL5-USP7 interaction, we expressed full-length human TSPYL5 in *E. coli* (SoluBL21) and purified the protein using nickel resin and size exclusion chromatography (SEC) (Fig. 2A). Two distinct forms were obtained: full-length TSPYL5 (TSPYL5 FL), eluting at 12.38 ml (peak 1), and a truncated form (TSPYL5 TR), eluting at 15.05 ml (peak 2). Both proteins were highly pure, as confirmed by SDS-PAGE (Fig. 2B). SEC analysis determined the molecular weight (MW) of TSPYL5 FL to be around 360 kDa, suggesting oligomer formation, while mass spectrometry indicated a 47 kDa mass (Fig. S2A). The truncated form (TSPYL5 TR, 1-195 residues) had a measured MW of 21 kDa, with a potential cleavage site identified (Fig. 2C, Fig. S2B-E). Structural predictions from AlphaFold2 (Jumper et al. 2021; Varadi et al. 2024) suggested that the truncated form (highlighted in pink on the grey TSPYL5 FL structure) is largely unfolded (Fig. 2D). Circular dichroism (CD) and nano differential scanning fluorimetry (nanoDSF) analysis revealed TSPYL5 FL exhibits at least partial folding, with an α-helical and β-sheet content (two minima near 208 nm and 222 nm) (Fig. 2E) and a melting temperature of 63.2°C (Fig. 2F). In contrast, TSPYL5 TR showed profiles typical of unfolded proteins, consistent with structural predictions (Fig. 2G, H).

To further probe TSPYL5 FL structure, we performed hydrogen-deuterium exchange mass spectrometry (HDx-MS) experiments. HDx-MS provides insights into solvent accessibility and secondary structure, as exchange rates vary with structural context: they are fastest in disordered regions (random coils), intermediate in α-helices, and slowest in β-sheets (Weis 2016). The HDx-MS data (Fig. 2I) revealed that most of TSPYL5 exchanges deuterium rapidly, suggesting a predominantly flexible and disordered conformation. However, variations in exchange rates were observed in regions predicted to form β-sheets and α-helices, largely aligning with the AlphaFold2 structural model. Notably, some discrepancies between the predicted and experimentally determined secondary structure were observed. For example, AlphaFold2 predicts a β-sheet for residues NSLEVEEL, whereas HDx-MS suggests that the β-sheet extends to residues (VL)SYLNSLEV, preceding the predicted region. Additional discrepancies can be deduced from Fig. S3.

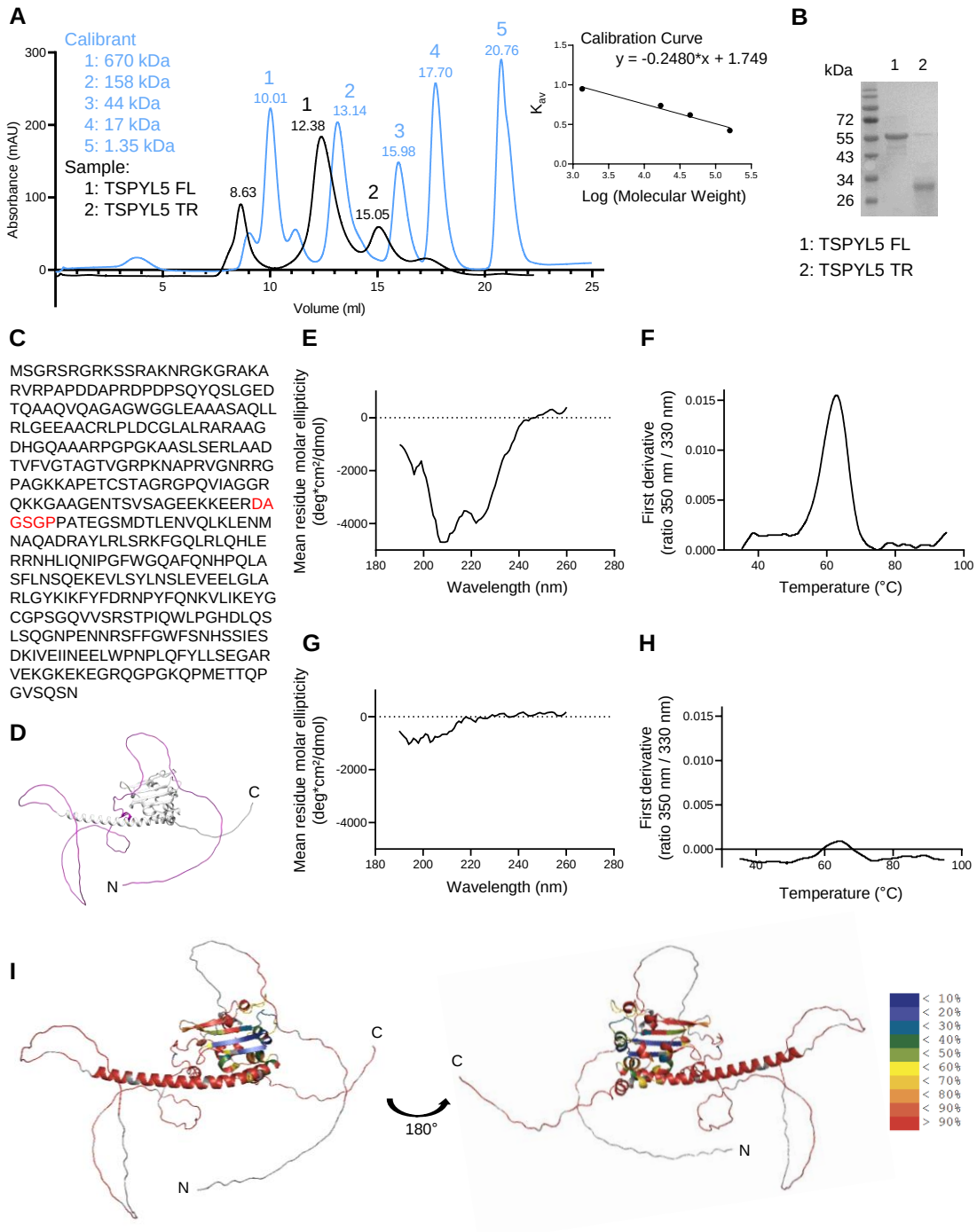

Figure 2: TSPYL5 adopts a partially structured conformation and spontaneously cleaves into a predominantly unfolded form. (**A**) Size exclusion chromatography (SEC) profile of TSPYL5 (black curve) during the purification process displays an elution volume of 12.38 ml (peak 1) (TSPYL5 FL), corresponding to an estimated molecular weight of ~360 kDa, based on a calibration curve (standard protein elution profile in light blue). A smaller species elutes at 15.05 ml (peak 2), corresponding to a

225 truncated form of TSPYL5 (TSPYL5 TR). Elution volumes are indicated above the peaks. The calibration
226 curve was generated using proteins of known molecular weight (K_{av} is the distribution coefficient, slope
227 SE = 0.02872, Y-intercept SE = 0.1254); the first peak of the calibration profile was excluded due to
228 exceeding the column's separation range. (**B**) SDS-PAGE analysis shows the molecular weights and
229 purity of TSPYL5 FL and TR eluting in peaks 1 and 2, respectively. (**C**) Mass spectrometry analysis
230 identifies the potential cleavage site (highlighted in red) on the TSPYL5 construct sequence (details in
231 Figure S2). (**D**) AlphaFold2 representation of TSPYL5 TR (highlighted in pink), corresponding to the N-
232 terminus of the full-length protein superimposed on TSPYL5 FL structure. "N" refers to the N-terminus
233 and "C" to the C-terminus. (**E**) Circular dichroism analysis of TSPYL5 FL (0.2 mg/ml). (**F**) Thermal
234 denaturation profile of TSPYL5 FL, measured by nano Differential Scanning Fluorimetry (nanoDSF)
235 (Melting Temperature = 63.2°C). (**G**) Circular dichroism analysis of TSPYL5 TR (0.2 mg/ml). (**H**) Thermal
236 denaturation profile of TSPYL5 TR, measured by nanoDSF (uncalculated Melting Temperature). (**I**)
237 Hydrogen-deuterium exchange mass spectrometry (HDx-MS) analysis of TSPYL5 FL. The H-D
238 exchange percentage at 60 s is mapped onto the AlphaFold2-predicted TSPYL5 structure. Color coding
239 indicates exchange dynamics: high exchange (red) denotes flexible, disordered regions, while lower
240 exchange suggests the presence of secondary structures, including β-sheets (blue) and α-helices
241 (yellow/green).

242

243 **Both TSPYL5 FL and TR bind strongly to USP7**

244 To investigate the interaction between TSPYL5 and USP7, we measured their binding
245 affinity using Microscale Thermophoresis (MST). Building on previous
246 immunoprecipitation data showing that the N-terminal half of TSPYL5 interacts with
247 USP7 in human cells, we used the naturally occurring truncated TSPYL5 (TSPYL5 TR)
248 form to further explore the role of the N-terminal region in mediating this interaction.
249 MST binding analyses confirmed that USP7 binds to full-length TSPYL5 (TSPYL5 FL),
250 with a dissociation constant (K_d) of 118.1 nM (Fig. 3A). In line with the cellular data,

TSPYL5 TR also demonstrated strong binding to USP7 with a K_d of 102.4 nM (Fig. 3B).

To validate these findings with an orthogonal method, we employed BioLayer Interferometry (BLI). Previous co-immunoprecipitation (co-IP) studies identified the MATH domain of USP7 as the key region mediating its interaction with TSPYL5 (Epping et al. 2011). Given that USP7 is a large protein, we decided to focus on its MATH domain (Fig. 3C). We successfully expressed and purified the USP7 MATH domain and confirmed its proper folding (Fig. S4A-D). In our initial BLI experiments, we attempted to titrate the MATH domain in solution using biotinylated TSPYL5 FL immobilized on streptavidin-coated sensors. However, we found that immobilizing TSPYL5 on the sensor likely obstructed its binding site, yielding inconclusive results (see supplementary material for more details, Fig. S5). In contrast, immobilization of the MATH domain after biotinylation produced clear and conclusive data (Fig. 3D and E). Kinetic analysis of TSPYL5 binding to the MATH domain revealed association (k_{on}) and dissociation (k_{off}) rates of around $1.3x10^{5}$ $M^{-1}s^{-1}$ and around $3.4x10^{-4}$ s^{-1}, respectively (Fig. 3F, Fig. S6), yielding a mean K_d of 3.4 nM. Similarly, the MATH domain exhibited comparable affinity for TSPYL5 TR, with a mean K_d of 2.1 nM.

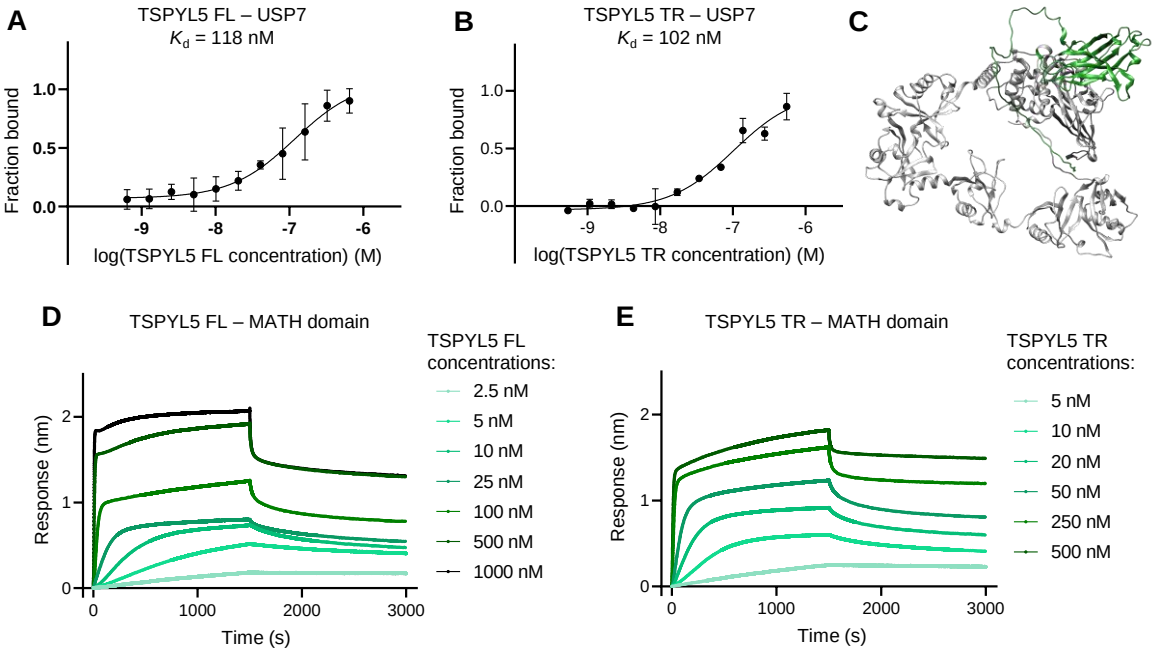

F

Protein immobilized on the sensor	Interacting partner	K_d from kinetic analysis
Biotinylated MATH domain	TSPYL5 FL	1.7 - 5.1 nM k_{on} = 7.0x10^4 - 1.9x10^5 1/M.s k_{off} = 3.2x10^{-4} - 3.6x10^{-4} 1/s
Biotinylated MATH domain	TSPYL5 TR	0.8 - 3.3 nM k_{on} = 7.2x10^4 - 2.1x10^5 1/M.s k_{off} = 1.7x10^{-4} - 2.4x10^{-4} 1/s

Figure 3: USP7 and its MATH domain interact strongly with both full-length and truncated TSPYL5. (**A**) Microscale thermophoresis binding curve for TSPYL5 FL, ranging from 650 nM to 0.635 nM, with a constant concentration of USP7 (100 nM), yields a dissociation constant (K_d) of 118 nM (95% CI [85 nM – 164 nM], N=3, mean ± SD). (**B**) Microscale thermophoresis binding curve for TSPYL5 TR, ranging from 550 nM to 0.537 nM, with USP7 at a constant concentration (100 nM), results in a K_d of 102 nM (95% CI [55 nM – 201 nM], N=2, mean ± SD). (**C**) AlphaFold2 prediction of the USP7 structure, highlighting the MATH domain in green in the N-terminal region. (**D**) Kinetic BioLayer Interferometry binding curves for TSPYL5 FL at various concentrations with a constant concentration of biotinylated

MATH domain (2.5 µg/ml). TSPYL5 FL is added at t = 0 s and washed at t = 1500 s. (**E**) Kinetic BioLayer Interferometry binding curves for TSPYL5 TR at various concentrations with a constant concentration of biotinylated MATH domain (2.5 µg/ml). TSPYL5 TR is added at t = 0 s and washed at t = 1500 s. (**F**) Determined affinity values for the binding of TSPYL5 FL and TR with the MATH domain of USP7 by BioLayer Interferometry (N=2; each value represents a replicate). See supplementary material for more details (Fig. S6).

Three key hotspots mediate the interaction between TSPYL5 and USP7

To investigate the primary interaction sites between TSPYL5 and USP7, we first identified key interaction regions within the TSPYL5 #1 and #2 sequences (Fig. 1C). We then conducted hydrogen-deuterium exchange mass spectrometry (HDx-MS) experiments with TSPYL5 and the MATH domain of USP7 to pinpoint specific interaction hotspots on the TSPYL5 sequence. This analysis covered 85.6% of the TSPYL5 sequence, enabling an in-depth examination of the binding across most of the protein (Fig. S7). Differential H-D exchange analysis revealed two major regions of TSPYL5 with significantly reduced deuterium uptake in the presence of the USP7 MATH domain. The first region spans residues ~210–262, while the second region covers residues ~368–388 at 15 and 60 s of exchange (Fig. 4A–B, Fig. S8–9).

To further refine the identification of interaction sites, we performed a peptide screening approach, which is particularly useful for mapping protein-protein interaction regions in unfolded proteins. We divided the 417 amino acids of TSPYL5 FL into 51 overlapping 17-amino-acid peptides, each overlapping by 9 residues, to ensure comprehensive sequence coverage (Fig. 4C). MST screening identified three overlapping peptides (peptides 9, 10, and 11) in the N-terminal region of TSPYL5 that bound to USP7, with dissociation constants (K_d) ranging from 12.6 µM to 500 µM (Fig.

4D–E, Table S2). These peptides map to amino acids 65–97 of TSPYL5, suggesting this region forms a key interaction hotspot. The localization of these three peptides within the TSPYL5 #1 sequence further supports the findings from cellular experiments. However, this region was not detected in HDx-MS experiments, presumably due to the very fast exchange kinetics in this region, which prevented the observation of differential deuterium exchange at the shortest time point tested (15 s), by which these peptides had already fully exchanged (Fig. S3).

Additionally, five interacting peptides were identified in the C-terminal region of TSPYL5 (Fig. 4D-F). The region corresponding to peptides 46 and 47 was also detected in HDx-MS, with these two peptides displaying low-affinity binding (Fig. 4D–F, Table S3). This low binding affinity may explain why TSPYL5 #3 failed to co-immunoprecipitate with USP7 in our cellular experiments. Among the five interacting peptides in the C-terminal region, only peptides 46 and 47 were validated by an orthogonal technique, designating them as confirmed interaction hotspots. The remaining peptides showed no detectable interaction, even at concentrations up to 1 mM (Fig. 4D, Table S2-3). Notably, no binding was observed for peptides from the first region identified by HDx-MS (residues ~210–262), likely due to the lack of a defined structural conformation of peptides, as this region is predicted to form an α-helix, which may be important for interaction. Overall, our experiments identified three key interaction hotspots: hotspot 1 in the N-terminal region (amino acids 65–97), hotspot 2 in the central region (amino acids 210–262) and hotspot 3 in the C-terminal region (amino acids 368–388).

To explore the evolutionary significance of the identified hotspots, we compared the human TSPYL5 sequence to those of other species (Fig. S10A). As expected, the NAP-like domain of TSPYL5 (underlined in orange) is highly conserved across

species. The three identified interaction hotspots (highlighted in pink) also displays notable conservation, suggesting their functional importance. A comparison of human TSPYL5 with other TSPYL family members (Fig. S10B) showed conservation of the NAP-like domain, whereas the N-terminal region, including the sequence corresponding to peptides 9, 10, and 11, exhibited significant divergence across family members. In contrast, the sequences corresponding to hotspots 2 and 3 displayed similarity across TSPYL family members, indicating potential functional overlap within the family.

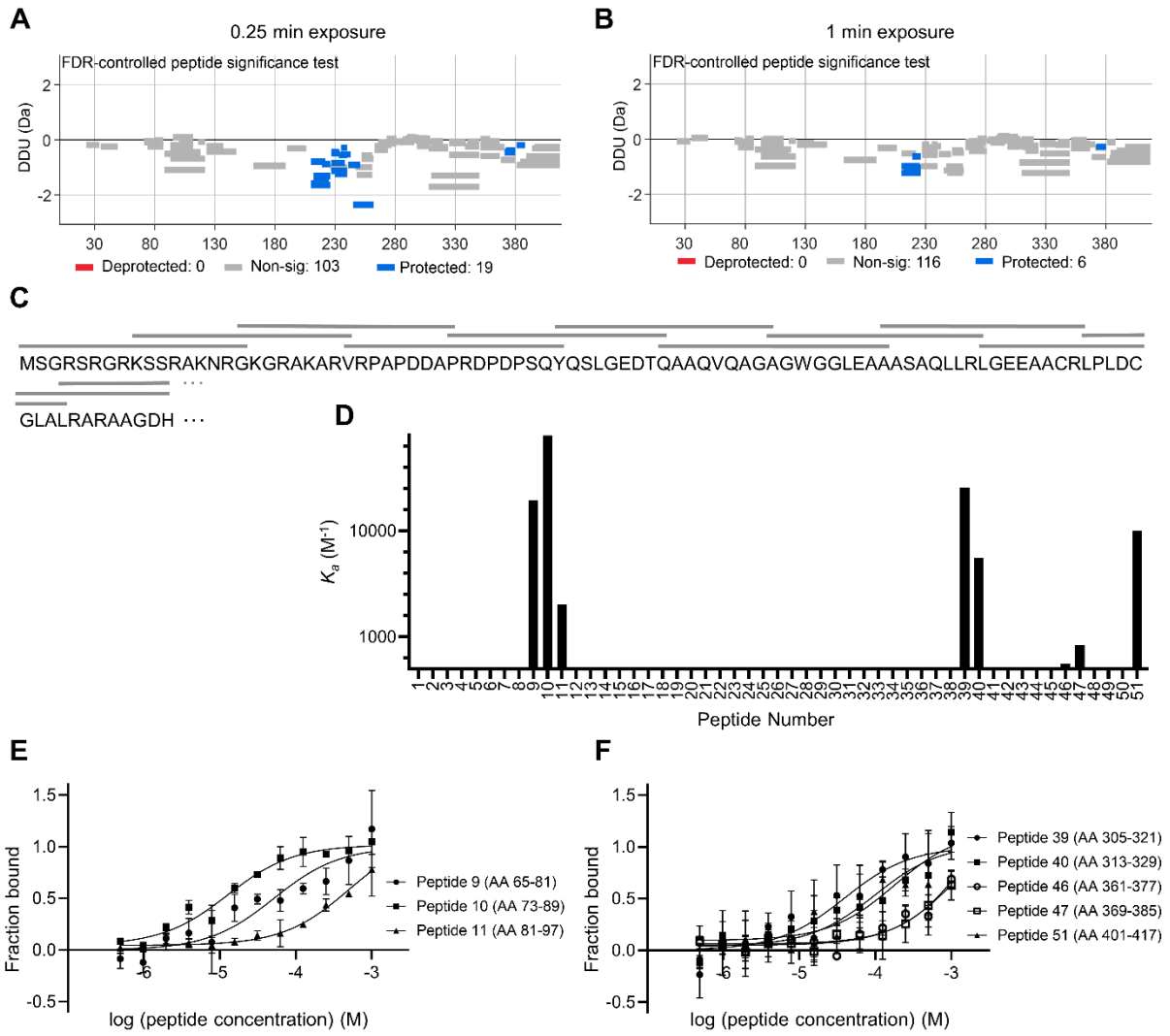

338

339 **Figure 4: Three key hotspots were identified for the TSPYL5-USP7 interaction.** (**A-B**) Differential
340 hydrogen-deuterium exchange (HDx) analysis identifies TSPYL5 peptides that exhibit protection or
341 deprotection upon MATH domain binding. Significantly protected peptides (peptide significance test, p
342 < 0.01 (Lau et al. 2021)) are shown in blue after 0.25 min (**A**) and 1 min (**B**) of deuterium exposure (FDR
343 = false discovery rate, DDU = differential deuterium uptake). (**C**) Schematic representation of the
344 TSPYL5 peptides used in the screening process, focusing on the N-terminal region of TSPYL5. Each
345 gray line represents an individual peptide. (**D**) Affinity constants (K_a = 1/K_d) obtained from Microscale
346 Thermophoresis (MST) for the 51 TSPYL5 peptides screened against USP7. USP7 concentration was
347 held constant (100 nM), while peptide concentrations ranged from 1 mM to 488 nM. Absence of a value
348 indicates undetectable binding (N=2 for most peptides, N=3 for interacting peptides; detailed data in
349 Table S2-3). K_a or K_d values for peptides 46 and 47 should be interpreted with caution, as the measured

350 K_d exceeds the highest tested peptide concentration. (**E-F**) MST binding curves for detected interacting
351 peptides shown in D, with amino acid boundaries indicated in parentheses (N=3, mean ± SD).

352

353 **TSPYL5 assembles into trimers and hexamers**

354 To further investigate TSPYL5, we performed negative staining electron microscopy,
355 which revealed a heterogeneous population of particles, predominantly around 9 nm
356 in size (Fig. 5A). This finding supports the high-MW species observed in our SEC
357 analysis (Fig. 2A). To explore the oligomerization mechanism, we conducted a
358 crosslinking assay with the BS^3 (Bis(Sulfosuccinimidyl) suberate) crosslinker. As the
359 crosslinker concentration increased, the monomeric TSPYL5 band gradually
360 disappeared, while multiple higher-MW bands appeared, indicating oligomer formation
361 (Fig. 5B). Due to the size and complexity of the resulting bands, precise MW
362 determination was challenging. Therefore, we used Dynamic Light Scattering (DLS)
363 and Mass Photometry (MP) for a more detailed analysis of TSPYL5 in solution. DLS
364 measurements showed that at higher concentrations (~50 µM), TSPYL5 forms 8 nm
365 complexes (Fig. 5C), consistent with the 9 nm particles seen in electron microscopy.
366 DLS also revealed a reduction in particle size as the protein concentration decreased
367 (Fig. 5C, Fig. S12A), aligning with the crosslinking data suggesting the existence of
368 multiple oligomeric states. Mass photometry, which provides accurate MW
369 determination at low concentrations (~ 80 nM), identified a trimer (~120 kDa) and its
370 dimerization to form a hexamer (~300 kDa) (Fig. 5D). Collectively, these results confirm
371 that TSPYL5 assembles into hexamers (~300 kDa, 8–9 nm in diameter) at higher
372 concentrations (~50 µM). Additionally, we observed that the hexamer formation occurs
373 via an intermediate trimer, which becomes more predominant at lower concentrations
374 (Fig. S12B).

To gain deeper insights into the oligomerization process of TSPYL5, we examined its truncated form (TSPYL5 TR, residues 1-195). Mass spectrometry determined its molecular weight (MW) to be 21 kDa, but size exclusion chromatography (SEC) analysis indicated a MW of ~65 kDa, suggesting trimer formation (Fig. 2A). To explore this further, we produced and purified an anti-truncated version of TSPYL5 (TSPYL5 anti-TR, residues 196-417) (Fig. S13A). Nano differential scanning fluorimetry (nanoDSF) analysis confirmed that TSPYL5 anti-TR is at least partially folded, with a melting temperature of 51.1°C (Fig. S13B). SEC analysis indicated an apparent MW of ~62 kDa, while its actual MW was ~28 kDa (Fig. S13C), suggesting dimerization. These findings imply that the N-terminal region of TSPYL5 plays a crucial role in trimer formation, while the C-terminal region likely mediates the interaction of two trimers, leading to hexamer formation.

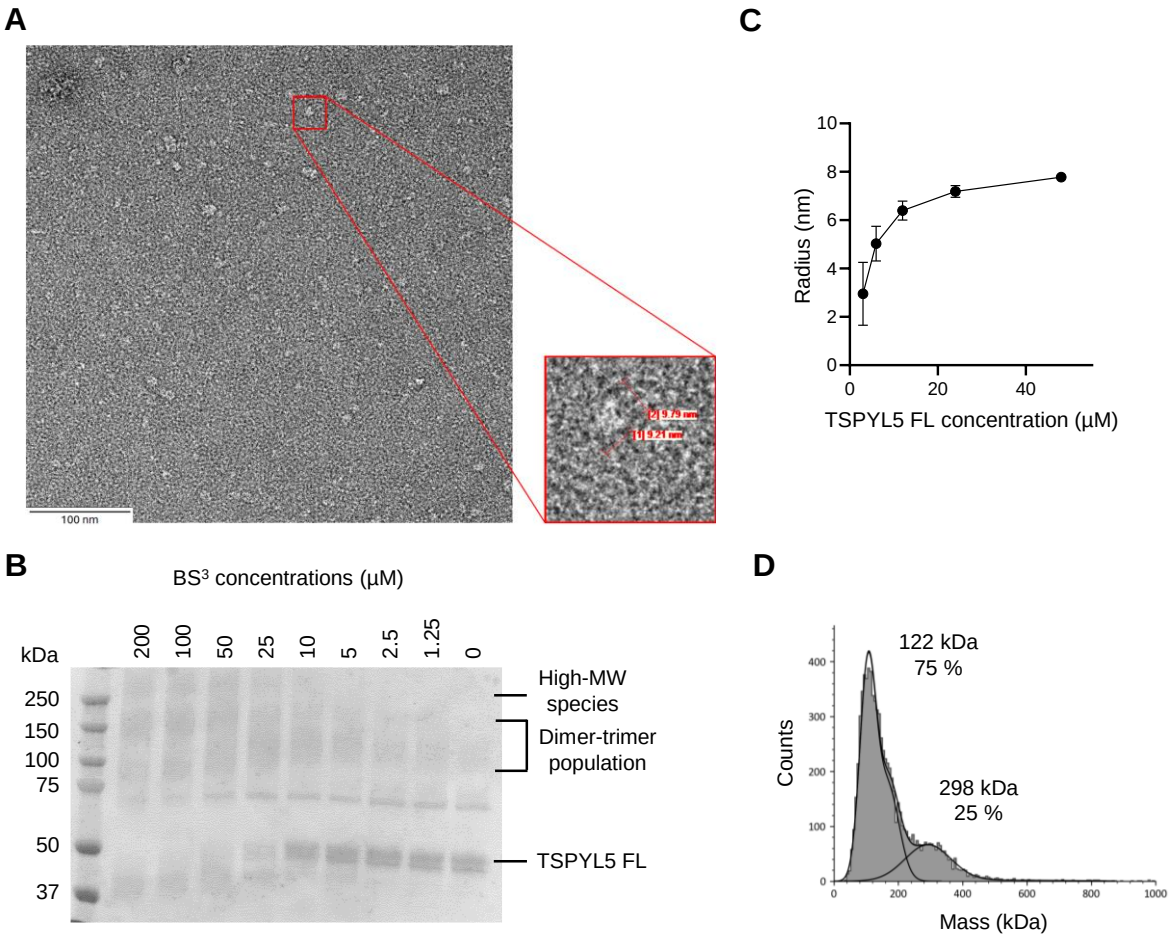

Figure 5: TSPYL5 forms trimers and hexamers. (**A**) Negative staining electron microscopy of purified TSPYL5 FL (0.01 mg/ml), with a zoom (in red) on a 9 nm diameter particle. (**B**) Crosslinking experiment: TSPYL5 FL was incubated at 3.5 µM with increasing concentrations of BS^3 and results were analyzed with SDS-PAGE. (**C**) Dynamic light scattering analysis of TSPYL5 FL at different concentrations (mean ± SD, N=2, n=6). (**D**) Mass photometry experiment of TSPYL5 FL at a low concentration (77 nM), with the calculated molecular weights of the complexes in solution and their relative abundance indicated next to the peaks.

DISCUSSION

The interaction between TSPYL5 and USP7 has emerged as a promising target for anti-ALT therapy, particularly in the context of pediatric cancers that rely on the ALT mechanism for telomere maintenance (Episkopou et al. 2019). However, the mechanistic details of this interaction remain poorly understood, limiting the development of effective therapeutic strategies. In this study, we characterized the interaction between full-length (FL) TSPYL5 and USP7, shedding light on key aspects of this interaction.

Our cell-based assays revealed that the N-terminal half of TSPYL5 mediates its interaction with USP7, while no binding was observed with the C-terminal half (residues 243–417), which includes the NAP-like domain. This suggests that the NAP-like domain does not play a significant direct role in USP7 binding. These findings were further supported by *in vitro* binding assays, confirming that the N-terminal region of TSPYL5, which is predicted to be disordered, is crucial for its interaction with USP7. Additionally, our binding hotspot analysis identified a specific interaction site within this

C-terminal region, albeit with low affinity, which likely explains why it failed to co-immunoprecipitate with USP7.

In line with previous studies (Silonov et al. 2024), our structural analysis confirmed that TSPYL5 is an intrinsically disordered protein, with its N-terminal region lacking a stable secondary structure. This structural flexibility likely contributes to its ability to engage in dynamic protein-protein interactions. Interestingly, we also observed the spontaneous formation of a truncated TSPYL5 form (TSPYL5 TR) during protein production, which we speculate reflects the structural instability of the full-length protein.

We used Microscale Thermophoresis (MST) to quantify the interaction between TSPYL5 and USP7, and the resulting dissociation constant of 118 nM for the full-length protein indicates high-affinity binding. The TSPYL5 TR form also exhibited similar binding affinity, suggesting that the interaction hotspot located within the disordered N-terminal region plays a major role in the binding. When we focused on the MATH domain of USP7, the binding affinity was even stronger (~3 nM), suggesting that the full-length USP7 may have structural constraints that reduce the accessibility of the MATH domain to TSPYL5. These results highlight the importance of the MATH domain in the TSPYL5-USP7 interaction and point to the need for further structural studies to understand how other USP7 domains may influence this interaction.

Peptide screening revealed a critical hotspot for the interaction between TSPYL5 and USP7 spanning amino acids 65 to 97 in the N-terminal region. However, hydrogen-deuterium exchange experiments failed to confirm this site, likely due to the rapid

exchange dynamics in this intrinsically disordered region, which prevented detectable differences under our experimental conditions. This region is highly conserved in TSPYL5 across species, suggesting its functional importance. Interestingly, the human TSPYL family members show some divergence in this region, which could explain why, except for TSPYL1 (Oughtred et al. 2021), they do not interact with USP7. This variability may indicate that the interaction between TSPYL5 and USP7 is specific to TSPYL5, while TSPYL1 may use distinct binding mechanisms.

Furthermore, our analysis of the TSPYL5 #2 fragment (residues 124–242) showed that it interacts with USP7 in cell-based assays. This was confirmed through HDx-MS experiments, which identified a binding hotspot within the α-helix spanning amino acids 210 to 262. However, no binding was detected in our *in vitro* peptide screening. This discrepancy suggests that the structured α-helix within this fragment may not be well-represented in the peptide screening model, as it does not preserve the native conformation of the full-length protein.

Previous studies have identified a consensus sequence (P/A/E-x-x-S) for the binding of the MATH domain of USP7 to various targets (Kim and Sixma 2017). The absence of this consensus in the identified TSPYL5 hotspots suggests that TSPYL5 interacts with USP7 via a unique mechanism. This is consistent with previous observations that TSPYL5 functions as an inhibitor of USP7, rather than as a substrate (Epping et al. 2011). Additionally, the fact that USP7 binds to some substrates at two distinct sites (Ma et al. 2010) further supports the idea that TSPYL5 may engage USP7 in a non-canonical manner, distinct from other USP7 substrates.

The unexpectedly similar K_d values observed for TSPYL5 TR and FL, despite the truncation occurring just before the α-helix, were intriguing. We speculate that a single,

strong binding hotspot in the N-terminal region could be sufficient to maintain the overall interaction, ensuring high affinity even in the absence of additional interaction sites. This hypothesis is further supported by the peptide screening results, where peptides 9, 10, and 11 exhibited lower K_d values compared to other identified peptides. Alternatively, the structural characteristics of TSPYL5 TR may enhance the accessibility or stability of this hotspot, leading to comparable binding affinities despite the truncated form having fewer interaction regions. This suggests that cooperative effects between different binding sites could contribute to the overall affinity, as previously suggested (de Vink et al. 2022).

We also observed that TSPYL5 forms oligomeric species in solution, with trimers and hexamers being the predominant forms at lower and higher concentrations, respectively. The N-terminal region appears to drive trimer formation, while the C-terminal region likely promotes hexamer formation by the interaction of two trimers. This oligomerization behavior is consistent with previous reports that the C-terminal region of TSPYL5 can self-assemble (Dalui et al. 2022), as well as with findings from related proteins like TSPY1, which require oligomerization for function (Shen et al. 2018). These results suggest that TSPYL5 may rely on oligomerization for its full functional activity, which could be an important consideration when developing targeted inhibitors.

In conclusion, this study provides a detailed characterization of the TSPYL5-USP7 interaction, identifying key binding hotspots and revealing the structural basis for this interaction. The high-affinity binding observed between TSPYL5 and USP7, particularly within the disordered N-terminal region, offers a promising target for the

development of specific inhibitors. These inhibitors could selectively kill ALT-positive cancer cells, potentially offering a more specific and less toxic therapeutic option. Furthermore, our findings on the oligomerization behavior of TSPYL5 open new avenues for designing strategies that target its oligomeric state. Together, these insights provide a strong foundation for the development of peptide- or small molecule-based inhibitors with minimal off-target effects, paving the way for the next generation of anti-ALT therapies.

MATERIALS AND METHODS

Chemicals and reagents. All reagents were obtained from commercial suppliers, as detailed below, and were used without further purification.

DNA constructs. The complementary DNA encoding TSPYL5 full length or different constructs was generated by PCR from the pBABE-puro-1×Flag-Nbio-TSPYL5 retroviral plasmid (Table S4) using forward and reverse primers (Table S5). The PCR products were subsequently cloned into the pCDNA-3×FLAG-NLS-TPP1 plasmid (Table S4). All final constructs were confirmed by DNA sequencing.

Cell culture. The *in vitro* immortalized human embryonic kidney cell line, HEK293T (ATCC CRL-3216), as well as the osteosarcoma cell line, U2OS (ATCC HTB-96), were cultured in DMEM (41965039, Gibco) supplemented with 10% FBS (F7524, Sigma-

Aldrich) and 1% penicillin-streptomycin (17602E, Lonza), under 37°C / 5% CO_2 conditions.

Transfection. Cells were seeded in 6-well plates with a density of 0.15 million cells/well and incubated overnight (ON) before transfection. Per well, 1 µg of plasmid (Table S4) and 4 µg of PEI 25K™ (23966, Polysciences Inc.) were mixed in 200 µL of serum-free medium (31985047, Gibco) and incubated at room temperature (RT) for 20 min before incubation with the cells for 6 h in 1.8 mL medium supplemented with 10% FBS. After the 6 h incubation, the medium was discarded and replaced with fresh supplemented medium.

Immunoprecipitations and western blotting. Cells were washed two times with ice-cold phosphate-buffered saline (PBS) and lysed for 30 min in NP-40 lysis buffer (50 mM Tris-HCl pH 7.4, 1 mM EDTA pH 8, 75 mM NaCl, 0.5 % NP-40) supplemented with protease inhibitors (11836153001, Roche). Lysates were centrifuged at 12,000 × g for 10 min at 4°C, supernatants were collected and heated for 10 min at 95°C in 6× Laemmli buffer (300 mM Tris-HCl pH 6.8, 60% glycerol, 12% sodium dodecyl sulphate (SDS) and 0.03% bromophenol blue, completed with 0.1 M dithiothreitol (DTT)). Alternatively, for immunoprecipitations, 500 µg of proteins were incubated overnight at 4°C with 20 µL of anti-Flag M2 affinity gel (A2220, Sigma-Aldrich). Immunoprecipitates were washed three times in cold NP-40 wash buffer (50 mM Tris-HCl pH 7.4, 1 mM EDTA pH 8, 75 mM NaCl, 0.1% NP-40), and beads were eluted and heated for 3 min at 95°C in 6× Laemmli buffer. Western blotting was performed according to standard procedures using antibodies described in Table S6. Revelation was performed with SuperSignal West Pico Chemiluminescent Substrate (ThermoFisher Scientific).

Proteins production and purification

TSPYL5. The nucleotidic sequence encoding TSPYL5, modified to include an N-terminal 6x histidine tag followed by a thrombin cleavage site, was cloned into the pET-28a expression vector and synthesized by Genecust. The recombinant plasmid was transformed into *Escherichia coli* SoluBL21 cells. Transformed *E. coli* cultures were grown in terrific broth (TB) supplemented with 50 µg/mL kanamycin at 37°C. Protein expression was induced by adding 1 mM isopropyl β-D-1-thiogalactopyranoside (IPTG) when the culture reached an optical density (OD_{600}) of 0.8. The cultures were incubated overnight at 20°C with shaking at 120 rpm. Cells were harvested by centrifugation at 5000 rpm for 25 min at 4°C (rotor 11150, Sigma) and resuspended in lysis buffer (50 mM Tris-HCl, pH 7.8, 0.5 M NaCl, 1 mM DTT, 25 mM imidazole, 0.1 mg/mL 4-(2-aminoethyl)benzenesulfonyl fluoride (AEBSF), 1 µg/mL leupeptin, 50 µg/mL deoxyribonuclease 1 (DN25, Sigma-Aldrich), 20 mM $MgCl_2$). The cells were lysed using a French® Pressure Cell Press (SLM-Aminco). The lysate was centrifuged at 10,000 rpm for 30 min at 4 °C (rotor 12165-H, Sigma), and the insoluble fraction was discarded. The recombinant protein was purified using a HisTrap™ FF crude column (1 mL, Cytiva) equilibrated with buffer containing 20 mM Tris-HCl, pH 7.8, 0.5 M NaCl, 1 mM DTT, and 25 mM imidazole. TSPYL5 was eluted with the same buffer containing 1 M imidazole. The eluted fractions were concentrated to a final volume of 500 µL and further purified by size-exclusion chromatography on a Superdex™ 200 Increase 10/300 GL column equilibrated with 20 mM Tris-HCl, pH 7.8, 0.5 M NaCl, and 1 mM DTT. Protein concentration was determined using the Bradford assay (Bio-Rad Protein Assay Dye Reagent), and purity was assessed by SDS-PAGE, followed by staining with InstantBlue Coomassie Protein Stain (Abcam). The purified protein was dialyzed

overnight to a buffer containing 20 mM Tris-HCl, pH 7.8, 0.5 M NaCl, 1 mM DTT, and 10% glycerol. Nano-differential scanning fluorimetry (nanoDSF) was performed using a Tycho NT.6 instrument (NanoTemper Technologies) in the dialysis buffer at a protein concentration of approximately 0.8 mg/mL to assess protein folding. Protein aliquots were stored at −80°C.

TSPYL5 anti-TR. The nucleotidic sequence encoding TSPYL5 anti-TR (residues 196-417 of TSPYL5 FL), modified to include an N-terminal 6x histidine tag followed by a thrombin cleavage site, was cloned into the pET-28a expression vector and synthesized by Genecust. The recombinant plasmid was transformed into *Escherichia coli* BL21-Gold cells. Transformed *E. coli* cultures were grown in terrific broth (TB) supplemented with 50 µg/mL kanamycin at 37°C. Protein expression was induced by adding 1 mM isopropyl β-D-1-thiogalactopyranoside (IPTG) when the culture reached an optical density (OD_{600}) of 0.8. The cultures were incubated overnight at 37°C with shaking at 130 rpm. Cells were harvested by centrifugation at 5000 rpm for 25 min at 4°C (rotor 11150, Sigma) and resuspended in lysis buffer (50 mM Tris-HCl, pH 7.8, 0.5 M NaCl, 1 mM DTT, 25 mM imidazole, 0.1 mg/mL 4-(2-aminoethyl)benzenesulfonyl fluoride (AEBSF), 1 µg/mL leupeptin, 50 µg/mL deoxyribonuclease 1 (DN25, Sigma-Aldrich), 20 mM $MgCl_2$). The cells were lysed using a French® Pressure Cell Press (SLM-Aminco). The lysate was centrifuged at 10,000 rpm for 30 min at 4°C (rotor 12165-H, Sigma), and the insoluble fraction was discarded. The recombinant protein was purified using a HisTrap™ FF crude column (1 mL, Cytiva) equilibrated with buffer containing 20 mM Tris-HCl, pH 7.8, 0.5 M NaCl, 1 mM DTT, and 25 mM imidazole. TSPYL5 was eluted with the same buffer containing 1 M imidazole. Protein concentration was determined using the Bradford assay (Bio-Rad Protein Assay Dye Reagent), and purity was assessed by SDS-PAGE, followed by staining with

InstantBlue Coomassie Protein Stain (Abcam). Nano-differential scanning fluorimetry (nanoDSF) was performed using a Tycho NT.6 instrument (NanoTemper Technologies) in a mix of wash and elution buffer at a protein concentration of approximately 6.5 mg/mL to assess protein folding. The purified protein was dialyzed overnight to a buffer containing 20 mM Tris-HCl, pH 7.8, 0.5 M NaCl, 1 mM DTT, and 10% glycerol. Protein aliquots were stored at −80°C. Purified proteins was further analyzed by size-exclusion chromatography on a Superdex™ 200 Increase 10/300 GL column equilibrated with 20 mM Tris-HCl, pH 7.8, 0.5 M NaCl, and 1 mM DTT for molecular weight evaluation.

USP7. USP7 was ordered from Biotechne (R&D systems) (E-519-025).

MATH domain of USP7. The nucleotidic sequence encoding the MATH domain, modified to include an N-terminal 6x histidine tag, was cloned into a pET-28a expression vector and synthesized by Genecust. The recombinant plasmid was transformed into *Escherichia coli* Rosetta (DE3) cells. Transformants were grown in terrific broth (TB) medium supplemented with 50 µg/mL kanamycin and 34 µg/mL chloramphenicol at 37°C. When the culture reached an optical density (OD_{600}) of 0.8, expression of the MATH domain was induced with 1 mM isopropyl β-D-1-thiogalactopyranoside (IPTG), followed by incubation overnight at 20°C with shaking at 120 rpm. Cells were harvested by centrifugation at 5000 rpm for 25 min at 4°C (rotor 11150, Sigma), and the cell pellet was resuspended in lysis buffer (50 mM Tris-HCl, pH 8.5, 300 mM NaCl, 10 mM $MgCl_2$, 5 mM imidazole, 10% glycerol), supplemented with a protease inhibitor cocktail (cOmplete™ ULTRA Tablets, Mini, EDTA-free, EASYpack, Roche). The cells were lysed by sonication. The lysate was centrifuged at 10,000 rpm for 30 min at 4°C (rotor 12165-H, Sigma), and the insoluble fraction was discarded. Beta-mercaptoethanol (1 µL/mL) was added to the supernatant. The

recombinant protein was purified using HisTrap™ FF crude columns (1 mL, Cytiva) pre-equilibrated with buffer containing 50 mM Tris-HCl, pH 8.5, 300 mM NaCl, 10 mM $MgCl_2$, 30 mM imidazole, and 10% glycerol. The MATH domain was eluted using 250 mM imidazole. Protein concentration was determined using the Bradford assay (Bio-Rad Protein Assay Dye Reagent), and purity was assessed by SDS-PAGE, followed by staining with InstantBlue Coomassie Protein Stain (Abcam). The purified protein was dialyzed overnight to a buffer containing 50 mM HEPES, pH 7.5, 100 mM NaCl, 1 mM TCEP, and 10% glycerol. Nano differential scanning fluorimetry (nanoDSF) was performed using a Tycho NT.6 instrument (NanoTemper Technologies) in the dialysis buffer at a protein concentration of approximately 1.2 mg/mL to confirm proper folding. Protein aliquots were stored at −80°C.

Peptides. All the peptides were ordered from ProteoGenix and were acetylated at their N-termini and amidated at their C-termini.

Protein characterization

Circular Dichroism. The buffer for purified full-length TSPYL5 and truncated TSPYL5 was exchanged to 20 mM sodium phosphate, pH 7.4, 200 mM NaF, and 1 mM DTT. Protein concentrations were determined using the Bradford assay (Bio-Rad Protein Assay Dye Reagent) for the truncated TSPYL5 and spectrophotometrically (Eppendorf BioSpectrometer) for the full-length TSPYL5. Both protein samples were diluted in the assay buffer to a final concentration of 0.2 mg/mL. Circular dichroism (CD) measurements were conducted at 25°C using a BioLogic MOS-500 spectropolarimeter (BioLogic, France) with a 1 mm path length quartz cuvette (#110-1-40, Hellma Analytics). Far-UV spectra were recorded from 190 to 260 nm with an acquisition

period of 0.5 s and steps of 1 nm. Five spectra were collected for each sample and averaged. Data analysis was performed using GraphPad Prism software.

Nano Differential Scanning Fluorimetry. Purified proteins were analyzed in their respective dialysis buffers using a Tycho NT.6 instrument (NanoTemper Technologies), following the standard manufacturer's protocol. Protein samples were loaded into capillaries and heated to 95°C over a period of 3 min. Fluorescence emission was monitored at 330 nm and 350 nm, following excitation at 280 nm. The instrument determined melting temperatures by calculating the derivative of the fluorescence intensity ratio (350/330 nm) as a function of temperature.

Dynamic Light Scattering. All samples and buffers were filtered using 0.2 µm filters to prevent contamination by particles. Dynamic light scattering (DLS) measurements were conducted using a DynaPro Dynamic Light Scattering Instrument (Wyatt Technology), and data were processed using DYNAMICS Basic Processing software (version 7.10.1.21). Samples were placed in specific DLS disposable microcuvettes (162960; Wyatt technology). Dilutions were performed directly in the cuvette by removing half of the sample volume and replenishing it with an equal volume of the storage buffer (20 mM Tris-HCl, pH 7.8, 0.5 M NaCl, 1 mM DTT, and 5% glycerol). Each sample was measured three times consecutively, with each measurement comprising five DLS acquisitions of 8 s each, separated by 1-s read intervals.

Negative Staining. Formvar carbon grids (EMS) were glow discharged using an ELMO glow discharger for 20 s at 4.5 mA. 3 µl of sample at 0.01mg/ml were applied to the grid and incubated for 30 s. After removal of the excess liquid, the grids were stained with 2% uranyl acetate solution (Zhang et al. 2013). After drying, the negative

stained grids were imaged using a JEOL1400 microscope equipped with a TVIPS F416 at 60,000x magnification.

Mass Spectrometry (MALDI-TOF). Matrix Assisted Laser Desorption Ionization – Time of Flight MS was acquired on a Ultraflextreme enhanced MALDI TOF/TOF-MS system (Bruker Daltonics, Bremen, Germany) using FlexControl 3.4 acquisition software (Bruker). For intact mass determinations, 1 µL of a 1:1:1 mixture of protein sample, 2.5 DHAP matrix (Bruker) and 2% v/v TFA was spotted in triplicate on an MTP ground steel plate. After crystallization, spectra were measured in the linear positive ion-mode within a mass range of 20,000 to 150,000 m/z. Up to 8000 shots were acquired with a laser repetition rate of 2000 Hz and 200 shots per rasterspot. All acquisition methods were provided by the manufacturer and optimized and calibrated with in-house made calibration standards (22 to 96 kDa, 4 calibrants). The obtained spectra were analyzed and processed (peak picking, smoothing and baseline substraction) with FlexAnalysis 3.4 (Bruker). Finally, the average of the three sample spots was taken to obtain the measured mass. For top down sequencing (TDS) experiments, 10 µL sample was mixed with 8 M GuHCl and desalted with a C18 ZIPTIP and eluted with a 50 mg/ml SDHB solution (dissolved in TA50). The eluent was diluted twofold with deionized water and 1.5 µL spotted on an MTP ground steel plate. All TDS experiments were measured in reflector and ion-positive mode within a range of 500 to 9000 Da with a by the manufacturer provided optimized acquisition method. Up to 12,000 shots were manually acquired and the used method was optimized and calibrated with an in-house made protein (15 kDa). The obtained spectra were processed and analyzed with FlexAnalysis 3.4 and BioTools 3.2.

Mass Photometry. Protein mass photometry was performed using a Refeyn OneMP system (Refeyn Ltd). The buffer, which was filtered prior to use, consisted of 50 mM

HEPES, pH 7.5, and 100 mM NaCl. Protein stock solutions at concentrations of 770 nM, 380 nM, and 190 nM were prepared, and 2 µL of each stock was directly added to an 18 µL drop of buffer on the measurement surface. Movies were recorded for 60 s (6000 frames) using the Acquire^{MP} software (version 2.1.1; Refeyn Ltd) under standard acquisition settings. Data analysis was conducted using Discover^{MP} software (version 2.1.1; Refeyn Ltd) with default settings. Prior to measurements, contrast-to-mass calibration was performed using a standard protein mixture with molecular weights of 66, 158, and 670 kDa.

Crosslinking. The buffer for purified full-length TSPYL5 was exchanged to PBS buffer (10.1 mM Na_2HPO_4, 1.7 mM KH_2PO_4, 2.7 mM KCl, 137 mM NaCl, pH 7.6). Proteins (3.5 µM) were incubated with varying concentrations of BS^3 cross-linker (ThermoFisher, #21580) for 30 min at room temperature. The cross-linking reaction was quenched by adding 50 mM Tris-HCl, pH 7, and incubating for an additional 15 min. Cross-linked protein samples were mixed with 1× Laemmli sample buffer (final protein concentration of 2.3 µM) and heated at 60°C for 10 min. The samples were then analyzed by SDS-PAGE, and the gels were stained using InstantBlue Coomassie Protein Stain (Abcam).

Microscale Thermophoresis. Microscale thermophoresis (MST) measurements were carried out using a NanoTemper Monolith NT.115 instrument (NanoTemper Technologies). USP7 was fluorescently labeled with a red dye–N-Hydroxysuccinimide (NHS) first-generation dye (NanoTemper Technologies), following the manufacturer's guidelines. All measurements were performed in premium-treated capillaries (NanoTemper Technologies) using buffer systems as follows: for TSPYL5 and truncated TSPYL5, the buffer composition was 95% buffer A (50 mM HEPES, 100 mM NaCl, 20% glycerol, 1 mM TCEP, 0.01% Tween 20, pH 7.5) mixed with 5% buffer B

(20 mM Tris-HCl, 0.5 M NaCl, 10% glycerol, pH 7.6); for peptide measurements, the buffer consisted of 50 mM HEPES, 100 mM NaCl, 20% glycerol, 1 mM TCEP, 0.01% Tween 20, pH 7.5. The final concentration of the fluorescently tagged protein was 100 nM. TSPYL5, truncated TSPYL5, or peptides were titrated using a 1:1 serial dilution. MST measurements were performed with 100% LED power and medium MST power, with a laser on time of 20 s and a laser off time of 3 s. Thermophoretic movement patterns were recorded, and dissociation constants (K_d) were calculated from the raw data at 2.5 s of MST on time, in accordance with the manufacturer's instructions, using MO.Affinity Analysis v2.3 software.

BioLayer Interferometry. Biolayer interferometry (BLI) measurements were conducted using an Octet® 96 system (Sartorius). Data were analyzed using FortéBio Data Analysis software (version 9.0.0.14) for reference subtraction, Savitzky–Golay filtering, and global fitting of the association and dissociation kinetic parameters. Proteins were biotinylated using EZ-Link™ NHS-LC-Biotin (Thermo Scientific, #21336) according to the manufacturer's instructions. Before the biotinylation, protein buffer was exchanged for PBS buffer through dialysis. NHS-LC-Biotin was prepared as a 10 mM stock solution in DMSO and incubated with protein samples at specific molar ratios (NHS-LC-Biotin:protein): 20:1 for the MATH domain and TSPYL5, and 1:1 or 0.1:1 for TSPYL5 optimization experiments. Incubations were conducted for 2 h on ice. Excess unreacted NHS-LC-biotin was removed by dialysis. The biotinylated proteins were immobilized onto streptavidin (SA) biosensors (Sartorius, #18-5019) at 2.5 µg/ml (except for NHS-LC-Biotin:TSPYL5 0.1:1 at 25 µg/ml) in a binding buffer composed of 50 mM HEPES, 100 mM NaCl, 20% glycerol, 1 mM TCEP, and 0.01 % Tween-20, pH 7.5. The interacting protein partner in solution was prepared at varying concentrations in the same buffer. As a negative control, the NemR protein (Kostyuk et al. 2022) was

biotinylated using the same protocol applied to other proteins, with a 20:1 molar ratio (NHS-LC-Biotin:protein). The biotinylated NemR was immobilized onto the same type of biosensors at a concentration of 2.5 µg/ml. The sensors were subsequently subjected to the same experimental conditions as those used for biotinylated MATH domain or TSPYL5, exposing them to various concentrations of either TSPYL5 or MATH domain. Binding responses recorded with biotinylated NemR were subtracted from the corresponding responses obtained with biotinylated MATH domain or TSPYL5 to eliminate non-specific binding signals. Association and dissociation phases were recorded in real-time. Data analysis was conducted using FortéBio Data Analysis software (version 9.0.0.14). Baseline adjustments, reference subtraction, and Savitzky–Golay filtering were applied, followed by global fitting to determine association and dissociation kinetic parameters.

Hydrogen Deuterium Exchange Mass Spectrometry. Hydrogen Deuterium Exchange Mass Spectrometry HDx-MS experiments were performed using a LEAP HDx Parralel MF system (Trajan) coupled to an UltiMate 3000 HPLC and an Orbitrap Fusion Lumos Tribrid Mass Spectrometer (Thermo Scientific). For the interaction between TSPYL5 and MATH, samples were mixed at a 1:1 ratio at 7.5 µM and stored at 0°C afterwards. 3.5 µl of proteins were diluted in 56.5 µl of equilibration buffer (5 mM K_2HPO_4, 5 mM KH_2PO_4 dissolved in H_2O, pH 7) for non-deuterated controls or in 56.5 µl labelling buffer (5 mM K_2HPO_4, 5 mM KH_2PO_4 dissolved in D_2O, pD 7) for 15, 60, 300, 900 or 3600 s. 50 µl of the exchange reaction was mixed with 50 µl of quench buffer (5 mM K_2HPO_4, 5 mM KH_2PO_4, 4 M urea for TSPYL5 analysis or 6 M urea for MATH analysis, pH 2.3) at 1°C. 90 µl of the quenched solution was directly injected in the LC-MS system. Samples were digested using a Nepenthesin-2/Pepsin mixed column (Affipro, AP-PC-006) at 10°C using a dynamic flowrate of 250-350 µl/min

gradient for 2 min for TSPYL5 and a fixed flowrate of 300 µl/min for MATH. Digested peptides were trapped captured on ACQUITY BEH C18 1.7 µm VANGUARD Pre-column (Waters), separated on a C18 5 µm 1.0 x 5 mm Vydak column at a flowrate of 25 µl/min with a linear gradient of H_2O/ACN 5-30% before being electrosprayed into a Orbitrap Fusion Lumos Tribrid Mass Spectrometer (Thermo Scientific). An EThcD fragmentation was applied for ions +2-+8 and a HCD fragmentation for ions +1 and +2. Peptides from undeuterated samples were identified using Proteome Discoverer 2.5. Peptides with XCorr > 2.0 were used as peptides pool for H-D exchange analysis. Hydrogen-deuterium exchange was calculated using HDExaminer. The deuteration levels were calculated based on the centroid of theoretical isotopes for all peptides. Each peptide was visually validated based on retention time and drift time. The results were further exported and analyzed with Deuteros 2.0 (Lau et al. 2021) using the peptide and hybrid significance test, as described (Lau et al. 2021). All time points and conditions were performed in triplicates.

SUPPLEMENTARY MATERIAL

- TSPYL5-USP7-supplementary-material. Supporting data contains figures and tables describing: Immunoprecipitation experiments in HEK293T cells, mass spectrometry results (intact mass analysis of TSPYL5 full-length and truncated, and Top-Down Sequencing Analysis of TSPYL5 truncated), hydrogen-deuterium exchange mass spectrometry (HDx-MS) analysis of TSPYL5 structure, MATH domain of USP7 purification results, BioLayer Interferometry optimization, BioLayer Interferometry data for MATH domain binding to biotinylated TSPYL5 (with different NHS-LC-Biotin:TSPYL5 molar ratio),

BioLayer Interferometry data with fitting curves for TSPYL5 full-length or truncated binding to biotinylated MATH domain, TSPYL5 sequence coverage in HDx-MS experiments, deuterium exchange results at extended exposure times, H-D exchange profile of selected peptides, TSPYL5 sequence comparison and hotspots localization, representation of the three identified interacting regions on TSPYL5 structure, dynamic light scattering and mass photometry complementary results, TSPYL5 anti-TR purification results and SEC analysis, secondary structure predictions based on circular dichroism results, peptides screened in MST for their binding to USP7 and measured K_d + Materials and Methods Tables describing plasmids, primers and antibodies used for Fig. 1 and Fig. S1.

- The complete raw data underpinning the results of this study can be obtained from the corresponding authors upon request.

ACKNOWLEDGMENTS

This work was supported by the Belgian Fonds National de la Recherche Scientifique (FNRS-EQP 31288018) and a Stichting tegen Kanker grant FAF-F/2018/1208 (to JM and AD). MA is a Research Fellow of the Belgian Fonds National de la Recherche Scientifique - FNRS. JM and KW were supported by a VIB grant. EK was supported by Excellence of Science project No. 30829584 granted to JM. JMP was supported by a FWO fellowship (1193524N). NP was supported by an Aspirant PhD fellowship from FSR-FNRS, Belgium. The hydrogen-deuterium exchange mass spectrometry platform

was supported by a grant from the Fondation Contre le Cancer awarded to Stefan N. Constantinescu (Advanced Technology Equipment n°3758).

We would like to thank Luis Fernando Durán Armenta for his help with DLS experiments. We would like to thank Attila Meszaros for helpful discussions during the preparation of the revised manuscript. We would like to thank the BECM VIB-VUB cryo-EM imaging facility in Brussels for support during imaging.

AUTHORS CONTRIBUTIONS

Marine Ancia: Conceptualization; methodology; data curation; validation; investigation; writing – original draft. **Khadija Wahni**: Methodology; data curation; validation; investigation; supervision. **Joudy Chakrowf**: Peptides screening; protein production. **Asia El Aakchioui**: Peptides screening; protein production. **Eloïse Claude**: Co-immunoprecipitation assay; data analysis; investigation. **Guillaume de Lhoneux**: Co-immunoprecipitation assay; data analysis; investigation. **Maxime Liberelle**: Methodology; validation; investigation; supervision. **Steven Janvier**: MS experiments; data analysis. **Ekaterina Baranova**: Structure analysis; validation. **Julia Malo Pueyo**: MP methodology; data curation; validation. **Ariana Jijon Vergara**: protein production. **Nicolas Papadopoulos**: HDx-MS experiments; data analysis; investigation. **Clémence Balty**: HDx-MS experiments; data analysis; investigation. **Jérôme Dejeu**: BLI methodology; validation; investigation; writing – original draft. **Anabelle Decottignies**: Conceptualization; validation; investigation; writing – review; project administration; supervision, resources. **Joris Messens**: Conceptualization; investigation; writing – review; supervision; resources. **Raphaël Frédérick**:

Conceptualization; validation; investigation; writing – review; project administration; supervision; resources.

REFERENCES

1. Hanahan D, Weinberg RA (2011) Hallmarks of cancer: The next generation. Cell 144(5):646-674.
2. Claude E, Decottignies A (2020) Telomere maintenance mechanisms in cancer: Telomerase, alt or lack thereof. Curr Opin Genet Dev 60:1-8.
3. Zhang JM, Zou L (2020) Alternative lengthening of telomeres: From molecular mechanisms to therapeutic outlooks. Cell Biosci 10:30.
4. Forrest SJ, Geoerger B, Janeway KA (2018) Precision medicine in pediatric oncology. Curr Opin Pediatr 30(1):17-24.
5. Episkopou H, Diman A, Claude E, Viceconte N, Decottignies A (2019) Tspyl5 depletion induces specific death of alt cells through usp7-dependent proteasomal degradation of pot1. Mol Cell 75(3):469-482 e466.
6. Epping MT, Meijer LA, Krijgsman O, Bos JL, Pandolfi PP, Bernards R (2011) Tspyl5 suppresses p53 levels and function by physical interaction with usp7. Nat Cell Biol 13(1):102-108.
7. Silonov S, Smirnov E, Shmidt E, Kuznetsova I, Turoverov K, Fonin A (2024) Insights into the cellular localization and functional properties of tspyl5 protein. International Journal of Molecular Sciences 25(39).
8. Dalui S, Dasgupta A, Adhikari S, Das C, Roy S (2022) Human testis-specific y-encoded protein-like protein 5 is a histone h3/h4-specific chaperone that facilitates histone deposition in vitro. J Biol Chem 298(8):102200.
9. Jumper J, Evans R, Pritzel A, Green T, Figurnov M, Ronneberger O, Tunyasuvunakool K, Bates R, Zidek A, Potapenko A et al. (2021) Highly accurate protein structure prediction with alphafold. Nature 596(7873):583-589.
10. Varadi M, Bertoni D, Magana P, Paramval U, Pidruchna I, Radhakrishnan M, Tsenkov M, Nair S, Mirdita M, Yeo J et al. (2024) Alphafold protein structure database in 2024: Providing structure coverage for over 214 million protein sequences. Nucleic Acids Res 52(D1):D368-D375.
11. Weis DD. 2016. Hydrogen exchange mass spectrometry of proteins: Fundamentals, methods, and applications.
12. Lau AM, Claesen J, Hansen K, Politis A (2021) Deuteros 2.0: Peptide-level significance testing of data from hydrogen deuterium exchange mass spectrometry. Bioinformatics 37(2):270-272.
13. Oughtred R, Rust J, Chang C, Breitkreutz BJ, Stark C, Willems A, Boucher L, Leung G, Kolas N, Zhang F et al. (2021) The biogrid database: A comprehensive biomedical resource of curated protein, genetic, and chemical interactions. Protein Sci 30(1):187-200.
14. Kim RQ, Sixma TK (2017) Regulation of usp7: A high incidence of e3 complexes. J Mol Biol 429(22):3395-3408.

15. Ma J, Martin JD, Xue Y, Lor LA, Kennedy-Wilson KM, Sinnamon RH, Ho TF, Zhang G, Schwartz B, Tummino PJ et al. (2010) C-terminal region of usp7/hausp is critical for deubiquitination activity and contains a second mdm2/p53 binding site. Arch Biochem Biophys 503(2):207-212.
16. de Vink PJ, Koops AA, D'Arrigo G, Cruciani G, Spyrakis F, Brunsveld L (2022) Cooperativity as quantification and optimization paradigm for nuclear receptor modulators. Chem Sci 13(9):2744-2752.
17. Shen Y, Tu W, Liu Y, Yang X, Dong Q, Yang B, Xu J, Yan Y, Pei X, Liu M et al. (2018) Tspy1 suppresses usp7-mediated p53 function and promotes spermatogonial proliferation. Cell Death Dis 9(5):542.
18. Zhang L, Tong H, Garewal M, Ren G (2013) Optimized negative-staining electron microscopy for lipoprotein studies. Biochim Biophys Acta 1830(1):2150-2159.
19. Kostyuk AI, Tossounian MA, Panova AS, Thauvin M, Raevskii RI, Ezerina D, Wahni K, Van Molle I, Sergeeva AD, Vertommen D et al. (2022) Hypocrates is a genetically encoded fluorescent biosensor for (pseudo)hypohalous acids and their derivatives. Nat Commun 13(1):171.